Technical Note

Landslides
DOI 10.1007/s10346-023-02089-5
Received: 2 November 2022
Accepted: 13 May 2023

Wei Lu · Yunfeng Hu · Zuopei Zhang · Wei Cao

A dual-encoder U-Net for landslide detection using Sentinel-2 and DEM data

Abstract Accurate and timely landslide mapping plays a critical role in emergency response and long-term land use planning. Deep learning–based methods represented by convolutional neural networks have been widely exploited in automatic landslide detection for their outstanding capability of feature representation and end-to-end learning mode. Most of the recent deep learning–based studies used toll-access high-resolution imagery for landslide detection. Considering demands for the future large-scale landslide mapping, this study aims to develop a new deep learning–based method to detect landslides using medium-resolution imagery and digital elevation model (DEM) data which are free-access and covered globally. Firstly, a workflow for constructing the landslide dataset is developed. Then, we design a semantic segmentation model to learn deep features and generate per-pixel landslide predictions. Specifically, the proposed network has a dual-encoder architecture with feature fusion to hierarchically represent deep features from the optical bands and DEM data. We also employ a self-attention module in the decoder of the proposed network to improve the performance. Experiments on two regions demonstrate that our method achieves the best F1 score of 79.24%, outperforming SegNet, U-Net, and Attention U-Net, the models popularly used in the semantic segmentation–based landslide detection. The proposed method may have an application potential in disaster risk assessment and post-disaster reconstruction and provide a technical reference for the large-scale landslide mapping in the future.

Keywords Landslide detection · U-Net · Semantic segmentation · Deep learning · Remote Sensing · Medium-resolution imagery

Introduction

Landslides are regarded as one of the most serious natural hazards and commonly occur in mountainous regions (Bacha et al. 2020; Mohan et al. 2021). Landslide triggers include natural events such as earthquakes, volcanic eruptions, intensive rainfalls, and climate change, as well as anthropogenic factors like urban sprawl, deforestation, underground mining, and constructing roads (McColl 2015). Landslides pose a significant threat to properties and human lives (Ye et al. 2019). Detecting landslides timely and promptly can support pre-disaster prevention, post-disaster relief, and long-term land-use planning (Puente-Sotomayor et al. 2021; Roccati et al. 2021). Traditional landslide detection methods based on field surveys usually consume a large amount of working time and financial resources. Remote sensing techniques are therefore considered primary research tools for rapid mapping of landslides.

Approaches for landslide detection based on remote sensing include visual interpretation (Zhang et al. 2019), change detection-based methods (Zhao et al. 2017b), knowledge-based methods (Martha et al. 2011; Keyport et al. 2018), machine learning methods (Ma et al. 2021; Wei et al. 2022), and deep learning methods (Mohan et al. 2021; Meena et al. 2022). Among these methods, visual interpretation is time-consuming and costly, requiring strong professional backgrounds for interpreters. Change detection–based methods require at least two satellite images photographed pre-event and post-event, respectively. However, due to weather conditions, it is often difficult to obtain available optical satellite images after landslides, especially those triggered by intensive rainfalls (Mondini et al. 2011). Synthetic-aperture radar (SAR) data is not affected by weathers, though landslide detection using SAR data usually obtained low accuracies (Liu et al. 2021b). Early researches used knowledge-based methods for landslide detection, such as threshold segmentation (Martha et al. 2011), object-oriented segmentation (Keyport et al. 2018; Bacha et al. 2020), and image enhancement (Yu and Chen 2017). However, knowledge-based methods have low transferability, because knowledge-based methods design rule sets typically for specific study areas (Bacha et al. 2020).

Machine learning (ML) classifies information automatically via model training, without man-designed classification rule sets (Ma et al. 2021). ML methods include support vector machine (Huang and Zhao 2018), random forest (Stumpf and Kerle 2011; Taalab et al. 2018), logistic regression (Wang et al. 2013; Budimir et al. 2015), and Bayesian classifier (Tsangaratos and Ilia 2016). For example, Tavakkoli Piralilou et al. (2019) integrated classification results computed by logistic regression, multi-layer perception, and random forest using Dempster-Shafer theory and obtained landslide inventory of Rasuwa, Nepal. The classification performance of ML methods is largely affected by the discernibility of input features. Thus, ML methods pose a high requirement for data preprocessing and feature engineering (Ma et al. 2021).

Deep learning (DL) has been widely applied in remote sensing image information extraction (Yuan et al. 2020), such as remote sensing scene classification (Tang et al. 2021; Peng et al. 2022), object detection (Sun et al. 2021; Zakria et al. 2022), and land use and land cover classification (Fitton et al. 2022; Zhu et al. 2022). DL methods outperform ML methods, because DL models can learn a hierarchical representation of data by layer-wise feature aggregation and message propagation, and extract discriminative high-level semantic features of remote sensing imagery (Yuan et al. 2020). DL methods for landslide detection can be grouped into object detection–based methods and semantic segmentation–based methods.

Object detection–based methods use bounding boxes to locate landslides. Object detection models in the computer vision domain, such as Region-based Convolutional Neural Network (R-CNN) series (Girshick 2015; Ren et al. 2015; He et al. 2017) and You-Only-Look-Once (YOLO) series (Redmon et al. 2016; Bochkovskiy et al.

2020), were used in landslide detection in recent studies. Ullo et al. (2021) exploited Mask R-CNN (He et al. 2017) to detect landslides using unmanned aerial vehicle images. Cheng et al. (2021) integrated an attention mechanism and YOLO v4 model to propose a small attentional YOLO (YOLO-SA) model for landslide detection. Object detection–based methods only label locations of landslides via rectangular boxes but not delineate exact boundaries of landslides.

Semantic segmentation–based methods aim to classify landslide pixels and non-landslide pixels to delineate locations, extents, and boundaries of landslides, belonging to the per-pixel segmentation task. Satellite imagery of high spatial resolution is commonly used in recent studies of semantic segmentation-based landslide detection (Yi and Zhang 2020; Chen et al. 2021a, b; Liu et al. 2021a; Su et al. 2021; Du et al. 2021; Yang et al. 2022; Yu et al. 2022). Du et al. (2021) built a landslide dataset which contained Google Earth images of 2.39-m spatial resolution mainly collected in the Jinsha River basin and corresponding per-pixel annotations. They conducted Fully Convolutional Network (FCN) (Long et al. 2015), U-Net (Ronneberger et al. 2015), Pyramid Scene Parsing Network (PSPNet) (Zhao et al. 2017a), Global Convolutional Network (GCN) (Peng et al. 2017), DeepLab v3 (Chen et al. 2017), and DeepLab v3 + (Chen et al. 2018) on their landslide database to verify the effectiveness of these semantic segmentation models on landslide detection task. Yi and Zhang (2020) proposed a new approach named as LandsNet for earthquake-triggered landslide detection, using RapidEye images of 5-m spatial resolution. They used 3 residential blocks for the encoding part and another 3 residential blocks for the decoding part and exploited the attention module proposed in Attention U-Net and multiscale fusion operations to improve performance. LandsNet outperformed Residential U-Net (ResU-Net) (Ronneberger et al. 2015; He et al. 2016) and Deep U-Net (Li et al. 2018) in their study areas. Yang et al. (2022) proposed CTransUNet which was modified from Transformer U-net (TransUNet) (Chen et al. 2021a, b) by exploiting the convolutional block attention module (CBAM) (Woo et al. 2018) in the decoder. The authors applied CTransUNet on landslide detection using Planet imagery of 3 m resolution and TripleSat imagery of 0.8 m resolution. Yu et al. (2022) proposed a hierarchical deconvolution network called as HADeenNet enabled with an attention module to enhance multi-scale features. They used HADeenNet on satellite imagery of up to 0.8 m resolution to detect landslides and obtained the best F1 score of 53.57%. Above semantic segmentation–based methods were mainly experimented on high-resolution imagery that is toll-access and with a low frequency of revisit. It is hard to collect accessible high-resolution images covered over the study areas for landslide rapid mapping.

In contrast, due to open access, global coverage, and frequent revisit of medium-resolution satellite imagery, using medium-resolution imagery for landslide mapping is a necessary part of future research on large-scale and long-term hazard information extraction. A few researchers (Ghorbanzadeh et al. 2021, 2022a; L. Bragagnolo et al. 2021) tried to use medium-resolution imagery to detect landslides. L. Bragagnolo et al. (2021) used Band 6, Band 5, and Band 4 of Landsat 8 imagery of 30 m resolution to map landslides in Nepal via U-Net, and they obtained an F1 score of 67%. Ghorbanzadeh et al. (2021) used Sentinel-2 imagery of 10 m resolution to detect landslides. They studied the performance and transferability of U-Net and ResU-Net on various landslide datasets and obtained the highest F1 score of 72.94%. Besides, multi-source data, such as digital elevation model (DEM), can help with landslide mapping since the development and movement of landslides are inextricably linked with terrains (Su et al. 2021). Ghorbanzadeh et al. (2022b) released a landslide benchmark data called Landslide4Sense by combining Sentinel-2 optical bands, slope data, and elevation data in 2022, which can promote the application of landslide detection and inspire further studies on mapping landslides using multi-source data. These studies mentioned above have tested the performance in landslide mapping using medium-resolution imagery of semantic segmentation models which originate from the computer vision domain, especially the U-shaped ones. However, compared with natural images or medical images used in the computer vision domain, remote sensing images have much more complicated scenes and abundant details so that it is harder to extract information from remote sensing images. There still exists space to design new methods in order to improve performance of landslide mapping using medium-resolution remote sensing imagery.

In all, our main objective is to propose a new semantic segmentation method for landslide detection using the open-access medium-resolution satellite imagery and DEM data. We design a dual-encoder architecture to learn deep features from the multi-source data and exploit a self-attention module to improve the performance. We compare the proposed method with other semantic segmentation models, i.e., SegNet, U-Net, and Attention U-Net to showcase the performance and potential of the proposed method for landslide detection using medium-resolution imagery.

Study area and data

Study area

Figure 1a shows the locations of the study areas in this paper. As presented in Fig. 1b, the first study area, the Wen-Du study area, is located at the junction of Wenchuan and Dujiangyan Counties of Sichuan province, China, with a total area of 334.06 km^2. It is near Chengdu city, the capital of Sichuan, and between 103°29′–103°40′E and 31°11′–31°20′N. Wen-Du study area belongs to the temperate humid climate zone. According to the yearbook released by the National Bureau of Statistics of China, in 2020 in Chengdu, the annual total precipitation is 1229.6 mm. The highest average monthly precipitation is 748 mm in August. This study area is located in the eastern edge zone of the Qinghai-Tibet Plateau. The elevation of the study area is 1029–4081 m, and the topography is predominated by mountains and deep valleys. The study area is on the east side of the Minjiang River and the west side of the Longmen Mountain, situated in the compound part of the Minjiang fault zone and Longmen mountain fault zone. The tectonic movements and rainfalls promote the formation of the landslides in this area.

As presented in Fig. 1c, the second study area, Iburi in short, is located in Iburi of Hokkaido, Japan, with a total area of 412.88 km^2. Iburi study area is between 141°53′–142°2′E and 42°41′–42°50′N, belonging to the temperate humid climate type. The study area is located in the frontal fold and thrust belt formed by the Hidaka Mountains, and the topography is predominated by low hills with the elevation of 16–449 m (Ozaki and Taku 2014; Zhang et al. 2019). Due to the active tectonic movements, the Iburi region was hit by an Mw 6.6 magnitude earthquake on September 6th, 2018. Besides, the Iburi region experienced persistent rainfalls before the

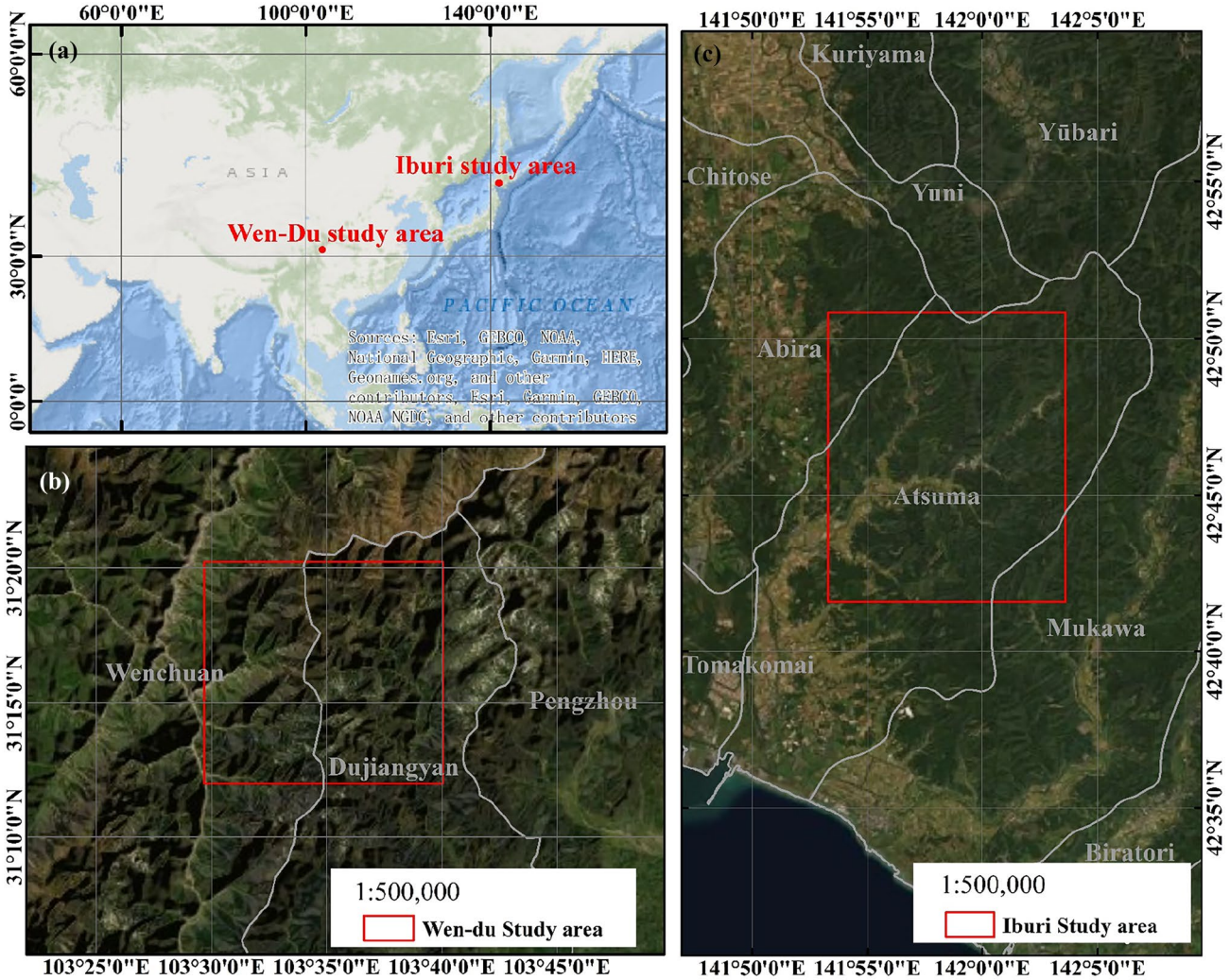

Fig. 1 Illustration of the study areas. **a** The locations of study areas, and the base map is the General Bathymetric Chart of the Oceans (GEBCO); **b** and **c** The zoom-ins of study areas, and the base map is ESRI World Aerial Imagery

earthquake. According to Zhang et al. (2019), from August 6th to September 6th, 2018, the cumulative precipitation almost reached 300 mm. Thus, the prolonged rainfall and the intense ground shaking resulted in the formation and sliding of thousands of landslides (Zhang et al. 2019).

Medium-resolution images and reference landslide inventories

In this paper, we collected Sentinel-2 images and NASA Digital Elevation Model (NASADEM) data for landslide detection. Sentinel-2 is a multispectral imaging mission with a wide swath and a global 5-day revisit frequency. The Sentinel-2 imagery has 13 bands of different spatial resolutions, with visible and near-infrared bands at 10 m resolution, red edge bands, and short wave infrared bands at 20 m resolution, and atmospheric bans at 60 m resolution. The NASADEM data is reprocessed from the Shuttle Radar Topography Mission data (JPL 2020). The NASADEM is at 30 m resolution.

Both Sentinel-2 and NASADEM data used in this study were freely collected and downloaded from Google Earth Engine using Python API and the GEEMap package (Wu 2020). In the Wen-Du study area, the rainy and cloudy weather in the mountainous region undermines the quality of optical images. Thus, we obtained the Sentinel-2 images collected in the summer half year (from March 1st to September 1st) in 2020, filtered them to metadata with a cloud pixel percentage of less than 30%, and applied cloud masks on the filtered images. Then, we generated a composite image via minimum values. The composite image has much better quality and fewer clouds than the single image. For the Iburi study area, we collected a Sentinel-2 image on August 6th, 2019 with the cloud pixel percentage less than 10%.

This study needed per-pixel reference landslide masks to train the further semantic segmentation network. For the Wen-Du study area, the multi-resolution segmentation method was performed by eCogniton software on Sentinel-2 images to generate objects, and then the object-oriented visual interpretation was conducted to

yield landslide masks. We further corrected the landslide masks with the help of Google Earth images. For the Iburi study area, we used the landslide database released by Zhang et al. (2019). The landslides covered an area of 13.35 km² in the Wen-Du study area and an area of 66.02 km² in the Iburi study area, respectively. The final reference landslide masks are binary data, of which "0" means background, and "1" denotes landslides. Figure 2 presents the Sentinel-2 images with RGB synthesis and corresponding landslide masks used in this study.

Method

Data preparation

According to the workflow of data preparation presented in Fig. 3, we first conducted re-projection on the obtained composite Sentinel-2 image and NASADEM data. The Sentinel-2 images and NASADEM data were re-projected by WGS 84/Pseudo-Mercator (ESPG: 3857) and resampled at 10 m resolution by the bilinear interpolation. The bilinear interpolation typically performs better than the nearest neighborhood method. Theoretically, higher-order interpolation methods, such as bi-cubic interpolation, may outperform the bilinear interpolation. However, considering both effectiveness and efficiency, we do not use higher-order interpolation methods because we believe the bilinear interpolation is enough for our data pre-processing. We do not compare the effectiveness of different interpolation methods since this is not the key component of our model.

Following Ghorbanzadeh et al. (2022b), we selected B1, B2, B3, B4, B5, B6, B7, B8, B9, B10, B11, and B12 from the Sentinel-2 imagery. Besides, we calculated the slope and aspect maps using the elevation data. Then, we totally collected 15 bands for landslide detection.

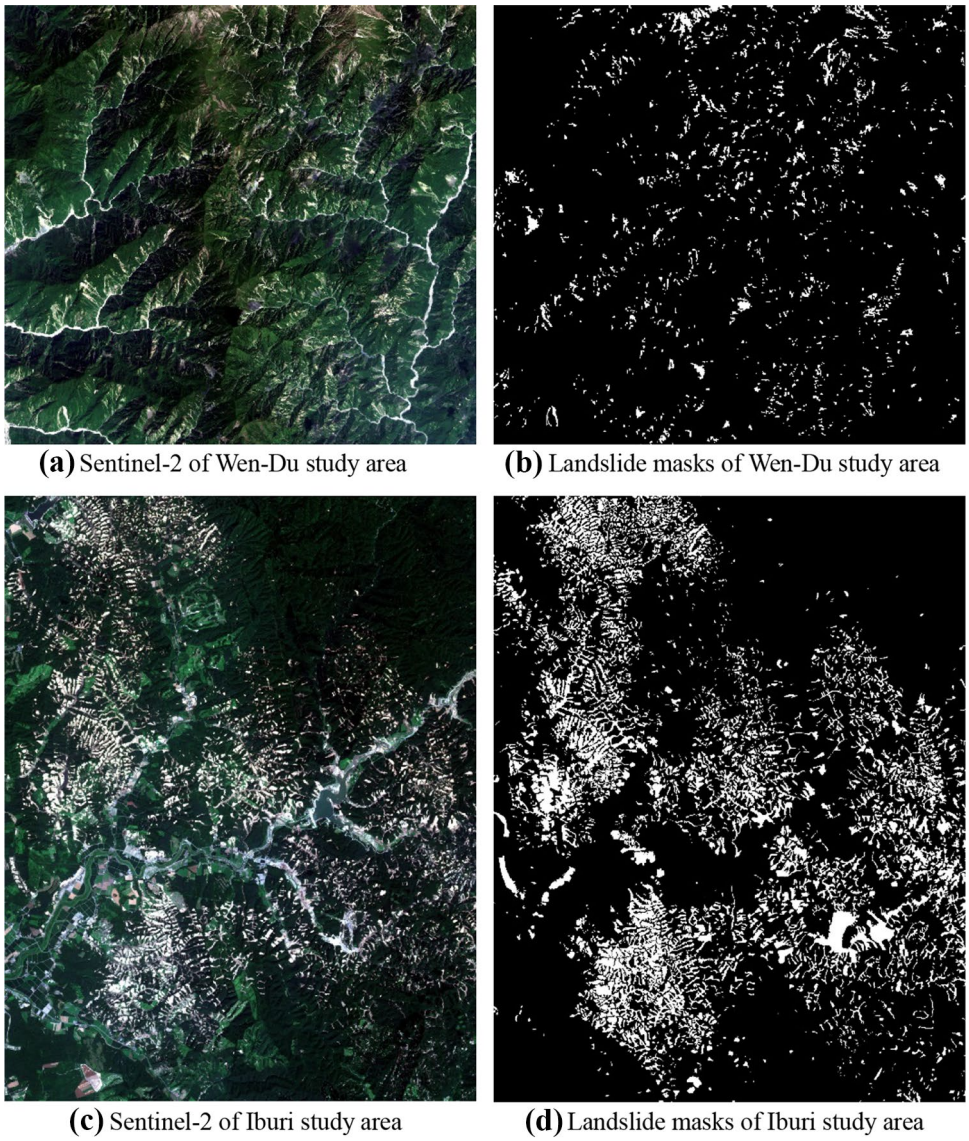

Fig. 2 Sentinel-2 images with RGB synthesis and ground truth landslide masks used in this paper

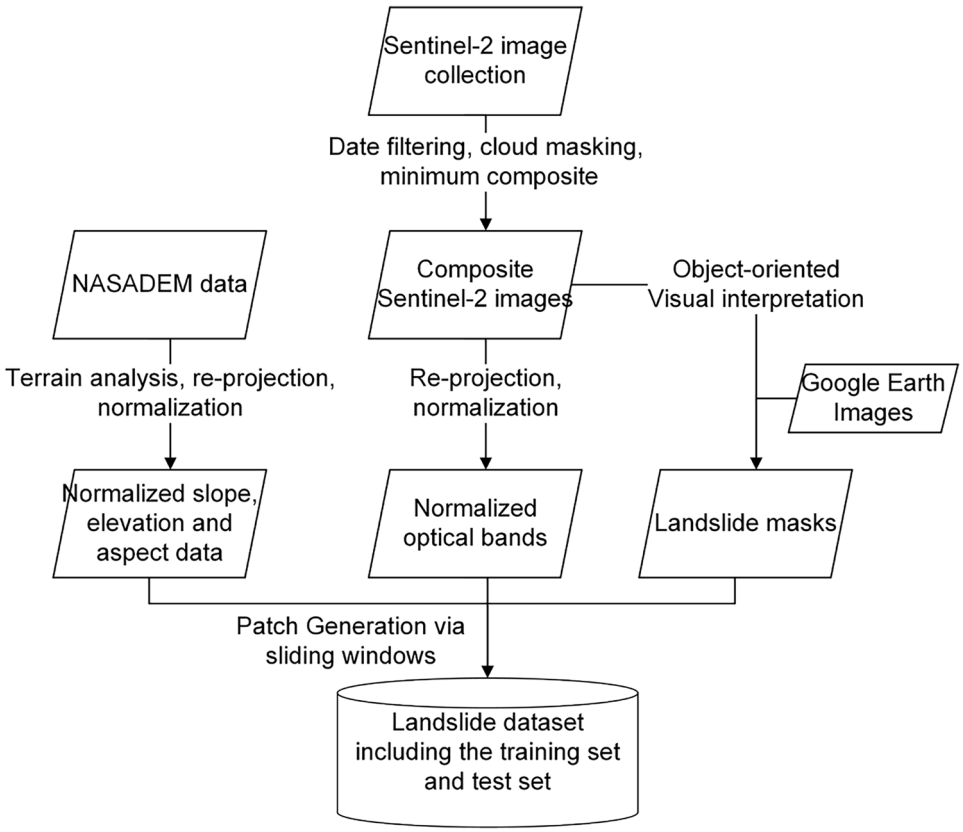

Fig. 3 The workflow for data preparation

Furthermore, we normalized the images to facilitate the proposed network training. Also following Ghorbanzadeh et al. (2022b), the bands were divided by a mean vector calculated from each channel to implement the normalization. The mean vector of the Wen-Du study area is 949.2088, 748.4695, 698.7444, 505.1842, 787.3141, 1267.6893, 1410.2332, 1399.5855, 755.9013, 17.6443, 941.9830, 557.1606, 30.8307, 2780.8990, and 175.2769, corresponding B1-B12, slope, elevation, and aspect. The mean vector of the Iburi study area is 1305.9524, 1018.6230, 914.6298, 670.2300, 955.5752, 2452.4155, 3165.0302, 2990.8410, 590.5851, 31.6564, 1714.7940, 791.9665, 13.7373, 162.7565, and 181.5565, corresponding B1-B12, slope, elevation, and aspect. The feature vector of pixels at each location is divided by the mean vector to generate the normalized feature vector.

As for the patch generation, we used a sliding window with the size of 128 × 128 pixels and a stride of 128 pixels to scan and clip the normalized data. Besides, corresponding label patches were obtained by scanning and clipping the per-pixel reference landslide masks.

Model building

In this paper, we propose a new landslide detection network, which is developed based on U-Net. As in Fig. 4, the proposed network consists of an encoding path and a decoding path, and a bridge connecting the encoding path and the decoding path. We design a dual-encoder architecture for jointly learning the deep semantic features in DEM data and optical bands and use a feature fusion strategy to integrate features in both encoders. In the decoding path, decoder blocks perform further optimization on features extracted by encoder blocks. The decoding part reconstructs spatial details of the targets layer by layer. A skip connection with an attention mechanism is used to fuse the output features of each decoder block with the output features of the corresponding encoder block. The network parameters are updated by jointly minimizing the cross-entropy loss with weights (Phan and Yamamoto 2020) and DICE loss (Milletari et al. 2016). Details of the proposed network are elaborated in the remaining part of this section.

Dual-encoding path with feature fusion In a deep semantic segmentation network, an encoder basically consists of convolutional layers, activation functions, and pooling layers. The convolutional layers learn deep features from the input data via linear convolutional operations. The computed results of linear convolutional layers are further sent to an elementwise activation function, such as rectified linear unit (ReLU) function to obtain feature maps. Parameters of convolution kernels are trainable and adaptively optimized by backward propagation. Pooling layers are used to down-sample feature maps in order to obtain high-level feature representation and reduce computational complexity. Commonly used pooling layers are maximum pooling and average pooling.

In the encoding path, we designed two encoders. One is the master encoder, consisting of four encoder blocks. The first

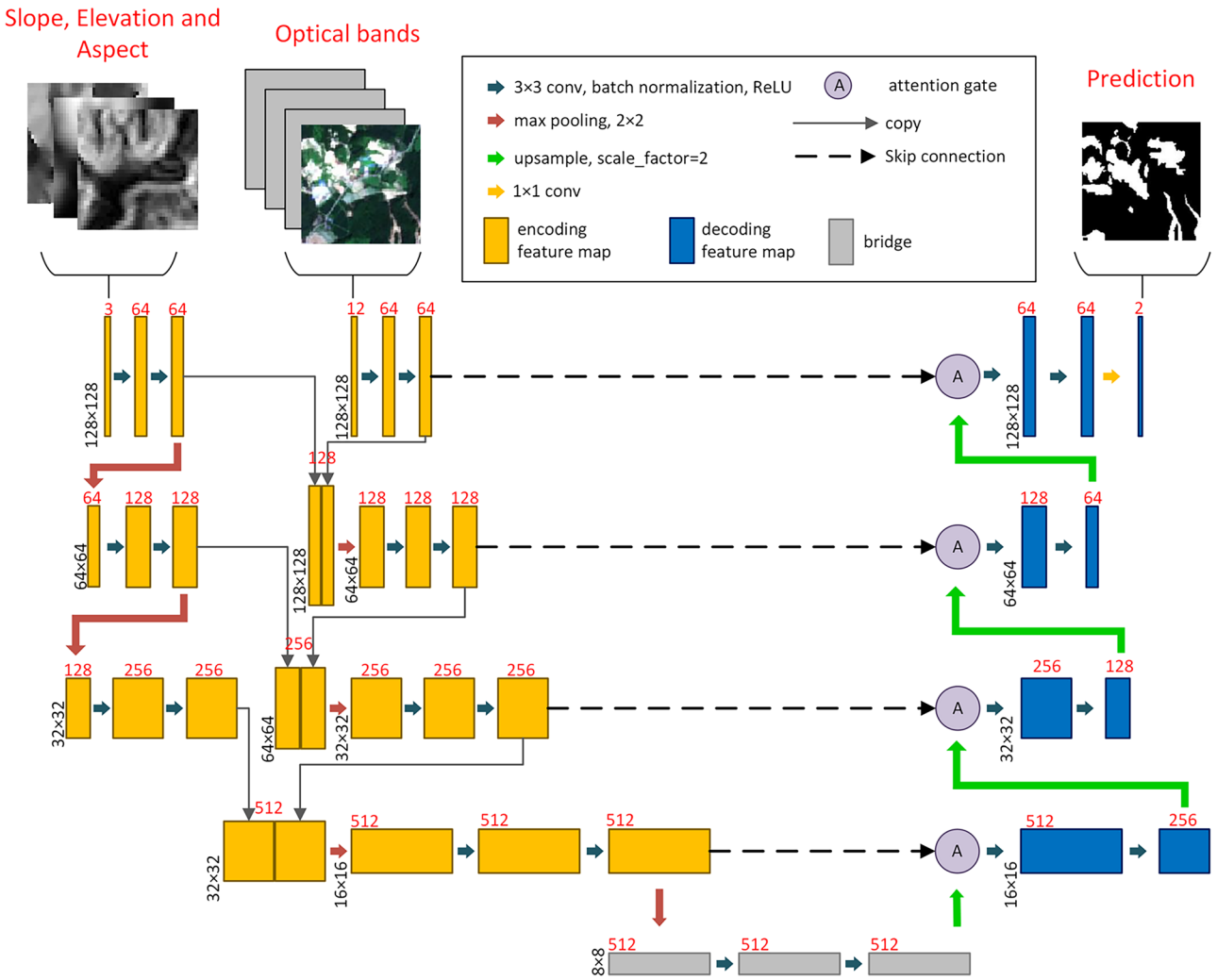

Fig. 4 The architecture of the proposed network for landslide detection using multiple optical bands and DEM data

encoder block of the master encoder contains two convolutional layers, and each of the followed three encoder blocks contains one pooling layer and two convolutional layers. Another encoder is the companion encoder, consisting of three encoder blocks. Each of the first two encoder blocks of the companion encoder has two convolutional layers and one pooling layer, while the third encoder block of the companion encoder only has two convolutional layers. Optical bands of the Sentinel-2 data are the input data of the master encoder, and DEM data is input to the companion encoder. Maximum pooling layers were used to aggregate deep information extracted by convolutional layers.

Meanwhile, features extracted from the two encoders are fused layer by layer. Specifically, feature maps from the corresponding encoder blocks respectively of the master encoder and the companion encoder were concatenated as the input of the next encoder block of the main encoder. The fusion strategy at the feature level helps to improve the feature expression capability and consistency of the network. The process of generating a feature map along the data flow in the master encoder is described as Eq. (1):

$$H_{\delta,l} = \sigma\left(BN\left(W_{\delta,2}\left(\sigma\left(BN\left(W_{\delta,1}\left(MaxPool_{2\times2}\left(H_{\vartheta,l-1} \parallel H_{\delta,l-1}\right)\right)\right)\right)\right)\right)\right) \quad (1)$$

where δ, ϑ denote the master encoder and the companion encoder, respectively; l is the serial number of the encoder block; m is the size of the feature map; $d(l)$ is the number of channels of the output feature map; $H_{\delta,l} \in \mathbb{R}^{m\times m\times d(l)}$ is the output feature map which is updated by the l th encoder block of δ, while $H_{\delta,l-1} \in \mathbb{R}^{2m\times 2m\times d(l-1)}$ is the output feature map calculated by the last encoder block of δ, and $H_{\vartheta,l-1} \in \mathbb{R}^{2m\times 2m\times d(l-1)}$ is the output feature map calculated by the last encoder block of ϑ. $\parallel$ represents feature concatenation. $W_{\delta,1} \in \mathbb{R}^{d(l)\times 2d(l-1)}$ and $W_{\delta,2} \in \mathbb{R}^{d(l)\times d(l)}$ are trainable parameter matrixes. BN denotes batch normalization, $\sigma(\cdot)$ denotes the activation function, and $MaxPool_{2\times2}(\cdot)$ is the maximum pooling operation.

The feature map generated by an encoder block in the companion encoder is computed as:

$$H_{\vartheta,l} = MaxPool_{2\times2}\left(\sigma\left(BN\left(W_{\vartheta,2}\left(\sigma\left(BN\left(W_{\vartheta,1}H_{\vartheta,l-1}\right)\right)\right)\right)\right)\right) \quad (2)$$

where $H_{\vartheta,l} \in \mathbb{R}^{m\times m\times d(l)}$ is the output feature map, $H_{\vartheta,l-1} \in \mathbb{R}^{2m\times 2m\times d(l-1)}$ is the input feature map, and $W_{\vartheta,1} \in \mathbb{R}^{d(l)\times d(l-1)}$ and $W_{\vartheta,2} \in \mathbb{R}^{d(l)\times d(l)}$ represent trainable parameter matrixes of the convolution layers of the encoder blocks. Besides the master encoder and the companion encoder, a bridge consisting of a maximum pooling layer, two convolution layers, and one up-sample layer is used to connect the encoding path and the decoding path.

Decoding path with attention A decoder commonly consists of up-sample layers and convolution layers. Up-sample layers resize the feature maps from the encoder, and then the resized feature maps are optimized by convolution layers. By stacking up-sample layers and convolution layers, the decoder reconstructs and highlights the object in the images. The proposed network contains four decoder blocks, and each decoder block has one up-sample layer and two convolutional layers to update features and adjust the number of feature channels. In the final decoder block, a 1×1 convolution layer is used to map classification results. At last, a feature vector with the length of the number of categories is generated at each pixel location.

U-shape networks universally adopt skip connection to use concatenation operation to fuse the features generated by the encoder and decoder at the same level, so that the decoder can retain more high-resolution details after up-sampling the feature maps. This study adopts a self-attention module proposed by Oktay et al. (2018) in the skip connection to fuse features better and to fascinate the model to focus on target information and inhibit useless background information. Figure 5 illustrates the self-attention mechanism.

In Fig. 5, X represents the up-sampled feature map from the decoder block; H represents the feature map from the corresponding encoder block; m is the size of feature maps; d_h and d_x denote the numbers of feature channels of H and X; d_int and d_out denote the numbers of intermediate feature channels and the output feature channels. H and X are first updated by 1×1 convolutional layers. Then the obtained feature maps are element-wise added together. The generated intermediate feature map is fed into another 1×1 convolutional layer to generate attention coefficients P. Furthermore, the input X is multiplied with P. Finally, the updated X with attention and the input H are concatenated to generate the output feature map.

Loss function The proposed network is trained with the joint loss function $\boldsymbol{L}$. $\boldsymbol{L}$ integrates weighted cross entropy loss function $\boldsymbol{L_{WCE}}$ and Dice loss function $\boldsymbol{L_{Dice}}$. The cross entropy function is easy to optimize while the Dice loss function aims to solve the problem of strong class imbalance. The integrated loss function $\boldsymbol{L}$ takes both advantages of cross entropy loss and Dice loss. $\boldsymbol{L}$ is computes as:

$$L = (1-\alpha)L_{WCE} + \alpha L_{Dice} \tag{3}$$

where $\alpha \in [0, 1]$ is a balance parameter. The weighted cross entropy loss is a variant of cross entropy loss (Phan and Yamamoto 2020), which is calculated as:

$$L_{CE} = -\frac{1}{N}\sum_{n=1}^{N}\sum_{k=1}^{K}\beta_k y_n \log\frac{\exp(\hat{y}_n)}{\sum_{j=1}^{K}\exp(\hat{y}_n)} \tag{4}$$

where N denotes the number of training samples, K denotes the number of classes, β_k is the weight value set for the k th class, y_n is the one-hot label of the n th sample, and $\hat{y}_n$ is the prediction of the n th sample. Weighted cross-entropy is useful for mitigating the problem of class imbalance (Phan and Yamamoto 2020).

Dice loss, originally from the Dice coefficient, was initially designed for the situation of strong class imbalance (Milletari et al. 2016). A Dice coefficient ranging between 0 and 1 is used to evaluate the similarity between two samples. Dice loss L_{Dice} is computed as:

$$L_{Dice} = 1 - \frac{2\left(\sum_{n=1}^{N} y_n \hat{y}_n\right)}{\sum_{n=1}^{N} y_n + \sum_{n=1}^{N} \hat{y}_n} \tag{5}$$

Performance assessment

We compute *precision*, *recall*, and F1 score (F1) to evaluate the performance of the proposed model. The three indexes are defined as:

$$precision = \frac{TP}{TP + FP} \tag{6}$$

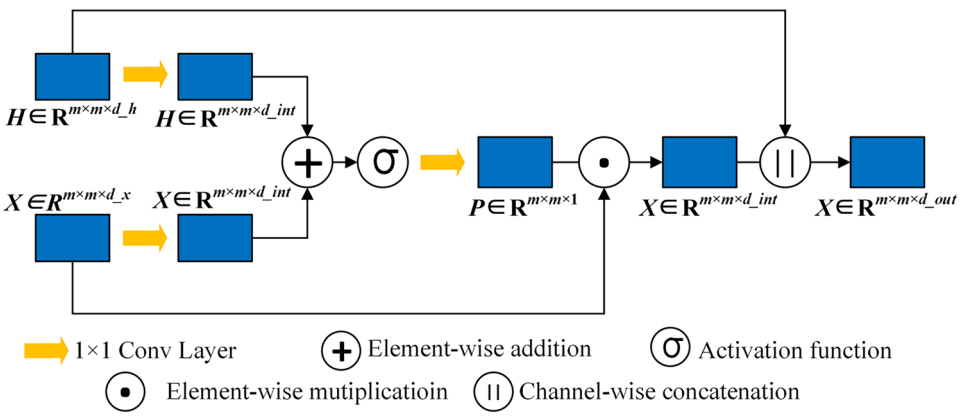

Fig. 5 Skip-connection with the self-attention module

$$recall = \frac{TP}{TP + FN} \tag{7}$$

$$\mathrm{F1} = \frac{2 \times precsion \times recall}{precsion + recall} \tag{8}$$

where TP is the number of true positives, i.e., pixels classified as landslides correctly; TN is the number of true negatives, i.e., pixels classified as backgrounds correctly; FP is the number of false positives, i.e., ground truth background pixels misclassified as landslides; FN is the number of false negatives, i.e., ground truth landslide pixels misclassified as backgrounds. *Precision* indicates the proportion of correctly classified landslide pixels from the predicted landslides. *Recall* indicates the proportion of correctly classified landslide pixels from ground truth landslides. F1 is regarded as the harmonic mean of *precision* and *recall* and can balance between *precision* and *recall*.

Experiments and results

Experimental settings

In this study, 210 and 252 image patches were generated for the Wen-Du study area and the Iburi study area, respectively. During model training, the image patches were randomly divided into the training set and the test set by the ratio of 7:3 in each study area. For the Wen-Du study area, 147 image patches were used for training and 63 for testing, while 176 image patches were for training and 76 for testing in the Iburi study area. Data augmentation, including random left–right flip and up-down flip, was performed on training sets for improving the robustness.

The output dimension of the model is set to 2. In terms of the weighted cross-entropy loss, the weight parameters for background and landslide, i.e., β_1 and β_2, were set to 0.5 and 1.0, respectively. The balance parameter of the joint loss function, i.e., α was set to 0.6. Adam was chosen as the model optimizer with a learning rate of 1e-3 and weight decay of 5e-4. The mini-batch size is 16. All the experiments were trained for 150 epochs. We also performed SegNet, U-Net, and Attention U-Net on the same study areas for comparison. All models were trained from scratch without using any pre-trained models.

Our experiments were implemented using PyTorch. All experiments were conducted on a personal computer equipped with an Intel core Xeon(R) Silver 4210R and NAVIDIA GeForce RTX 3090 GPU with 24 GB memory.

Description of processed data

Figure 6 presents 10 image patches that are preprocessed from Sentinel-2 images and DEM data as depicted in the "Data preparation" section. In Fig. 6, the first four rows represent four image patches in the Wen-Du study area, and the last six are from the Iburi study area. Each layer is in the size of 128 × 128 pixels. Bands B1-B12 are from the Sentinel-2 data. Bands B13-B15 are slope, elevation, and aspect calculated from DEM data, respectively. The mask is the ground truth of landslides.

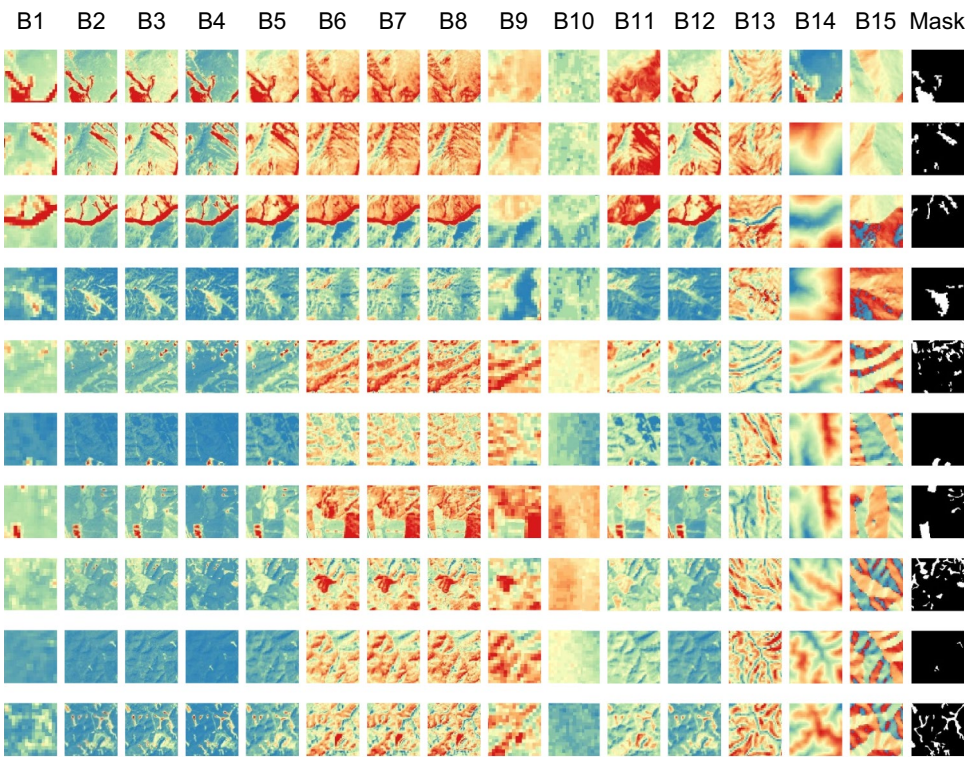

Fig. 6 Examples in the study areas of the processed data

Table 1 Quantitative results (%) in the Wen-Du study area

Model	Precision	Recall	F1-score
SegNet	46.84	52.15	49.35
U-Net	68.45	62.99	65.60
Att U-Net	63.20	71.37	67.04
Proposed Network	68.05	70.36	69.18

The dataset used in this paper has a strong class imbalance. In the training set of the Wen-Du study area, landslide pixels take up 4.44% of total pixels while in its test set, landslide pixels take up 3.03%. In the training set of the Iburi study area, landslide pixels take up 16.10% of total pixels while in its test set landslide pixels take up 15.73%. Thus, landslide detection is difficult in the Wen-Du study area due to the small volume of positive samples.

Experimental results

As presented in Table 1, our proposed network achieved the best landslide detection results according to the quantitative comparisons. Specifically, the proposed network achieved promising precision and recall scores, i.e., 68.05% and 70.36%, respectively, as well as keeping a good balance between the precision and recall. Among all of the comparison networks, SegNet generated the lowest precision and recall scores, indicating the high fraction of false positives and false negatives produced by SegNet. U-Net obtained the highest precision score, though it generated a relatively low recall score of 62.99%, which demonstrated that a large fraction of landslide pixels was wrongly classified as non-landslide pixels in the prediction produced by U-Net. Attention U-Net achieved the highest recall score, though it generated a relatively low precision score of 63.20%, indicating a large fraction of non-landslide pixels wrongly categorized as landslides in the predicted results. In addition, the proposed network obtained the highest F1 score of 69.18%, exceeding the second-highest F1 score generated by Attention U-Net by 2.14%. Figure 7 presents the results of four regions of the Wen-Du study area. In the figure, black indicates the background, red indicates true positives, cyan indicates false negatives, and yellow indicates false positives.

The quantitative comparisons in Table 2 also demonstrate that our network obtained the best classification results in the Iburi study area. The proposed network achieved the highest F1 value by 79.24%, exceeding SegNet, U-Net, and Attention U-Net by 5.57%, 2.66%, and 1.95%. Moreover, the proposed network kept a great balance between the precision and the recall, with the difference between the two indexes of 1.72%. Among the networks in Table 2, SegNet obtained the second-highest recall score but the lowest precision score, which demonstrated that SegNet generated a large number of false positives. In contrast, U-Net obtained the highest

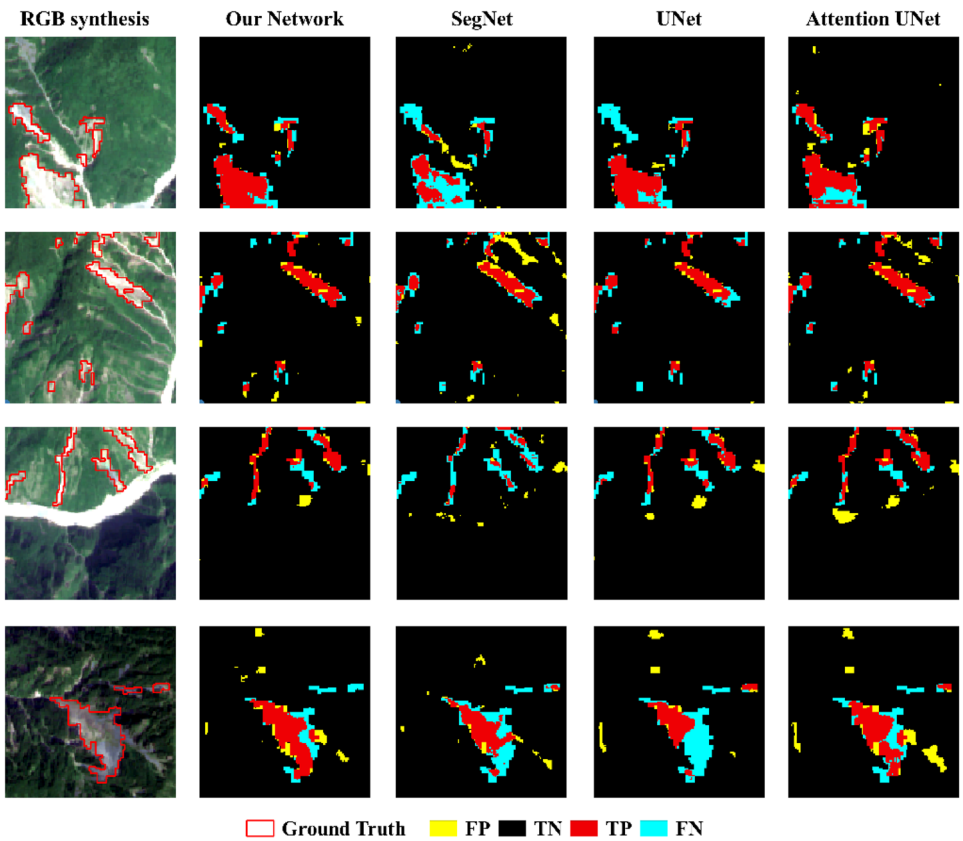

Fig. 7 Landslide detection results generated by our network, SegNet, U-Net, and Attention U-Net in 4 regions of the Wen-Du study area

Table 2 Quantitative results (%) in the Iburi study area

Model	Precision	Recall	F1-score
SegNet	71.67	75.57	73.57
U-Net	83.21	70.93	76.58
Att U-Net	82.50	72.69	77.29
Proposed Network	78.39	80.11	79.24

precision value but the lowest recall value, with the difference between the two indexes of 12.28%. Attention U-Net obtained the precision score of 82.50% and the recall score of 72.69%, with the difference between the two indexes of 9.81%. Generally considering the precision, the recall, and the overall accuracy, our proposed network achieved the best performance for detecting landslides in Iburi. Figure 8 presents the predicted results in 7 regions of Iburi.

Discussion

Comparison between the proposed network and previous work

In this paper, we obtained satisfactory results on landslide detection using free-access Sentinel-2 imagery and NASADEM data. Compared with studies using the toll-access with < 10 m resolution (Yi and Zhang 2020; Chen et al. 2021a, b; Liu et al. 2021a; Yang et al. 2022), our method is easier and has more potential to deploy in the future large-scale landslide detection tasks. It is worth noting that our method obtained the F1 score of 79.24% in the Iburi study area, and Yang et al. (2022) obtained an F1 of 79.33% using Planet imagery

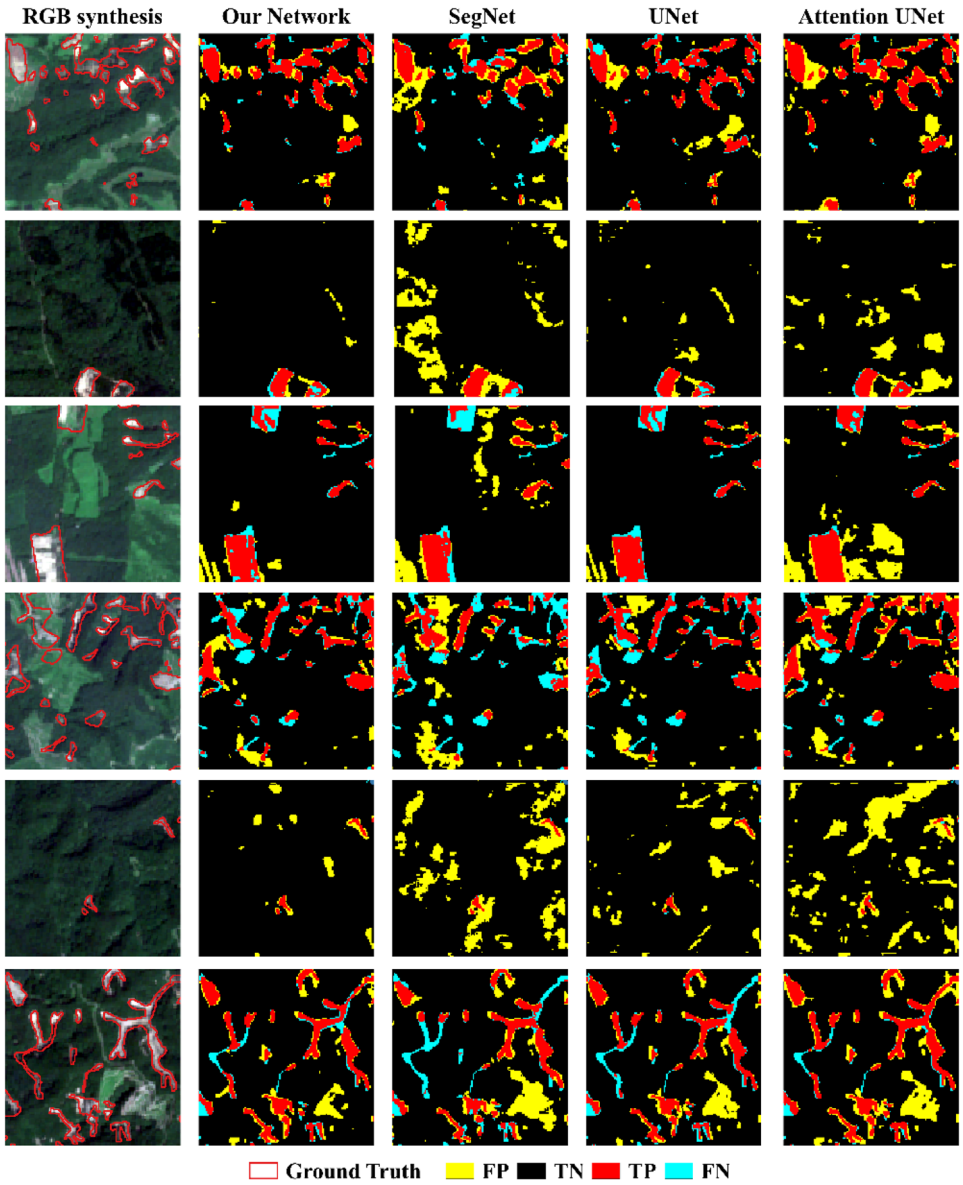

Fig. 8 Landslide detection results generated by our network, SegNet, U-Net, and Attention U-Net in 6 regions of the Iburi study area

of 3 m spatial resolution in the same study area. The small difference between the two demonstrated that our method performs well in landslide detection using medium-resolution and multi-spectral imagery and DEM data.

Previous studies (Ghorbanzadeh et al. 2021, 2022b; Bragagnolo et al. 2021) generally committed to explore the feasibility of deep learning models originating from the compute vision domain on landslide detection using medium resolution imagery. This study, in contrast, proposed a new network for landslide detection. The proposed network was proved to outperform the popularly used SegNet, U-Net, and Attention U-Net. In the Wen-Du study area, our model achieved an F1 score of 69.18%, which exceeded SegNet, U-Net, and Attention U-Net by 19.83%, 3.58%, and 2.14%. In the Iburi study area, our model achieved an F1 score of 79.24%, which exceeded the three comparison models by 5.67%, 2.66%, and 1.95%. Besides, our method kept a good balance between precision and recall.

In this study, we designed a dual-encoder architecture to extract high-level semantic features from optical bands and DEM data, respectively. We also introduced a self-attention module into the decoder. Compared with Attention U-Net, our method obtained better detection accuracies, which verified the effectiveness of our dual-encoder architecture.

Limitations, challenges, and future work

Deep learning models usually require a large number of training samples to improve robustness. Actually, research on landslide detection based on remote sensing is hampered by the lack of ground truth data, the arduous acquisition of accurate samples, and class imbalance. Researchers often need to expend considerable effort and resources on manual interpretation or field surveys to obtain accurate labeling data for model training. This study obtained 147 and 176 image patches in the size of 128×128 pixels for model training, which are actually relatively small training sets for deep learning. According to the experimental results, our method is impacted by the limited training samples and strong class imbalance. We performed data augmentation and modified the loss function for model training to alleviate the above issues, though. Thus, in the future, more accurate samples are needed for larger-range landslide detection. Other learning schemes, such as transfer learning and meta learning, are also worth exploring for landslide mapping using a few samples. Besides, limited by the paper length, we do not clarify the different contributions of each band to landslide detection. In our future study, it is necessary indeed to perform an ablation analysis on different Sentinel-2 bands.

Conclusion

In this paper, we proposed a semantic segmentation-based approach for landslide detection using Sentinel-2 imagery and DEM data. The main contributions of this study lie in that (1) we developed a method using medium-resolution remotely sensed imagery and DEM data to achieve accurate landslide mapping, which has the potential to deploy on large-scale landslide detection, and (2) the proposed method is per-pixel and end-to-end and outperforms the universally used SegNet, U-Net, and Attention U-Net in our study area.

In this paper, Sentinel-2 imagery and DEM data were preprocessed first to generate image patches for model training. Then we designed a dual-encoder U-Net with a self-attention module for landslide detection. The proposed network has two encoders, a main encoder to learn deep features from optical bands and a companion encoder to learn deep features from DEM data. The features learned by two encoders were fused. The decoder part of our network used a skip connection with an attention gate in order to suppress background information and pay more attention to target information.

We conducted experiments in the Wen-Du study area and the Iburi study area by comparing our network with SegNet, U-Net, and Attention U-Net. The quantitative evaluations showed that our network reached 69.18% of F1 in Wen-Du and 79.24% of F1 in Iburi. In both study areas, our network outperformed the compared networks. Moreover, qualitative comparisons of classification results generated by different networks also verify the effectiveness of the proposed network. Limited by bottlenecks including small sample size and class imbalance, the proposed network has only been experimented on in two study areas. Conducting more extensive landslide detection studies in the future will pose a greater challenge to the construction of the ground truth database. Future research on larger-scale, business-oriented landslide detection will pose greater challenges to the construction of landslide databases and the design of deep learning models.

Acknowledgements

We thank all the authors for their great contribution to this study. We also thank the editor and anonymous reviewers for their helpful suggestions.

Author contribution

Conceptualization: Yunfeng Hu; methodology: Wei Lu, Yunfeng Hu; formal analysis and investigation: Wei Lu; writing—original draft preparation: Wei Lu; writing—review and editing: Wei Lu; Yunfeng Hu, Zuopei Zhang, Wei Cao; visualization: Wei Lu; project administration: Yunfeng Hu; funding acquisition: Yunfeng Hu; supervision: Yunfeng Hu, Wei Cao. All authors have read and agreed to the published version of the manuscript.

Funding

This research was supported by the Network Security and Information Program of the Chinese Academy of Sciences (CAS-WX2021SF-0106), the National Natural Science Foundation of China (42130508) and the Key Project of Innovation LREIS (KPI011).

Availability of data and code

The Sentinel-2 imagery and NASADEM data are freely downloaded from Google Earth Engine platform at the website of https://developers.google.com/earth-engine/datasets/catalog/ (accessed on October 27, 2022). The ground truth of Iburi study area can be downloaded at the website of https://zenodo.org/record/2577300#.YzKiSXZByUl (accessed on October 27, 2022). The code used during the current study is available from the corresponding author on reasonable request.

Declarations

Conflict of interest The authors declare no competing interests.

References

Bacha AS, Van Der Werff H, Shafique M, Khan H (2020) Transferability of object-based image analysis approaches for landslide detection in the Himalaya Mountains of northern Pakistan. Int J Remote Sens 41:3390–3410. https://doi.org/10.1080/01431161.2019.1701725

Bragagnolo L, Rezende LR, da Silva RV, Grzybowski JMV (2021) Convolutional neural networks applied to semantic segmentation of landslide scars. CATENA 201:105189. https://doi.org/10.1016/j.catena.2021.105189

Bochkovskiy A, Wang C-Y, Liao H-YM (2020) Yolov4: Optimal speed and accuracy of object detection. arXiv preprint. arxiv.org/abs/2004.10934

Budimir MEA, Atkinson PM, Lewis HG (2015) A systematic review of landslide probability mapping using logistic regression. Landslides 12:419–436. https://doi.org/10.1007/s10346-014-0550-5

Chen F, Chong Xu, Wang L et al (2021b) Matrix SegNet: a practical deep learning framework for landslide mapping from images of different areas with different spatial resolutions. Remote Sensing 13:3158. https://doi.org/10.3390/rs13163158

Chen J, Lu Y, Yu Q et al (2021a) Transunet: transformers make strong encoders for medical image segmentation. arXiv preprint. arxiv.org/abs/2102.04306

Chen L-C, Papandreou G, Schroff F, Adam H (2017) Rethinking atrous convolution for semantic image segmentation. arXiv preprint. arxiv.org/abs/1706.05587

Chen L-C, Zhu Y, Papandreou G et al (2018) Encoder-decoder with atrous separable convolution for semantic image segmentation. In: Proceedings of the European conference on computer vision (ECCV). pp 801–818

Cheng L, Li J, Duan P, Wang M (2021) A small attentional YOLO model for landslide detection from satellite remote sensing images. Landslides 18:2751–2765. https://doi.org/10.1007/s10346-021-01694-6

Du B, Zhao Z, Hu X et al (2021) Landslide susceptibility prediction based on image semantic segmentation. Computers & Geosciences 155:104860. https://doi.org/10.1016/j.cageo.2021.104860

Fitton D, Laurens E, Hongkarnjanakul N et al (2022) Land cover classification through Convolutional Neur-al Network model assembly: a case study of a local rural area in Thailand. Rem Sens App Soc Environ 26:100740. https://doi.org/10.1016/j.rsase.2022.100740

Ghorbanzadeh O, Crivellari A, Ghamisi P et al (2021) A comprehensive transferability evaluation of U-Net and ResU-Net for landslide detection from Sentinel-2 data (case study areas from Taiwan, China, and Japan). Sci Rep 11:1–20. https://doi.org/10.1038/s41598-021-94190-9

Ghorbanzadeh O, Shahabi H, Crivellari A et al (2022a) Landslide detection using deep learning and object-based image analysis. Landslides 19:929–939. https://doi.org/10.1007/s10346-021-01843-x

Ghorbanzadeh O, Xu Y, Ghamisi P et al (2022b) Landslide4Sense: reference benchmark data and deep learning models for landslide detection. arXiv preprint, arxiv.org/abs/2206.00515. https://doi.org/10.48550/arXiv.2206.00515

Girshick R (2015) Fast r-cnn. In: Proceedings of the IEEE international conference on computer vision. pp 1440–1448

He K, Gkioxari G, Dollár P, Girshick R (2017) Mask r-cnn. In: Proceedings of the IEEE international conference on computer vision. pp 2961–2969

He K, Zhang X, Ren S, Sun J (2016) Deep residual learning for image recognition. In: Proceedings of the IEEE conference on computer vision and pattern recognition. pp 770–778

Huang Y, Zhao L (2018) Review on landslide susceptibility mapping using support vector machines. CATENA 165:520–529. https://doi.org/10.1016/j.catena.2018.03.003

JPL N (2020) NASADEM Merged DEM Global 1 arc second V001. NASA EOSDIS Land Processes DAAC

Keyport RN, Oommen T, Martha TR et al (2018) A comparative analysis of pixel-and object-based detection of landslides from very high-resolution images. Int J Appl Earth Obs Geoinf 64:1–11. https://doi.org/10.1016/j.jag.2017.08.015

Li R, Liu W, Yang L et al (2018) DeepUNet: a deep fully convolutional network for pixel-level sea-land segmentation. IEEE Journal of Selected Topics in Applied Earth Observations and Remote Sensing 11:3954–3962. https://doi.org/10.1109/JSTARS.2018.2833382

Liu T, Chen T, Niu R, Plaza A (2021a) Landslide detection mapping employing CNN, ResNet, and DenseNet in the Three Gorges Reservoir, China. IEEE Journal of Selected Topics in Applied Earth Observations and Remote Sensing 14:11417–11428. https://doi.org/10.1109/JSTARS.2021.3117975

Liu X, Zhao C, Zhang Q et al (2021b) Three-dimensional and long-term landslide displacement estimation by fusing C-and L-band SAR observations: a case study in Gongjue County, Tibet, China. Rem Sens Environ 267:112745. https://doi.org/10.1016/j.rse.2021.112745

Long J, Shelhamer E, Darrell T (2015) Fully convolutional networks for semantic segmentation. In: Proceedings of the IEEE conference on computer vision and pattern recognition. pp 3431–3440

Ma Z, Mei G, Piccialli F (2021) Machine learning for landslides prevention: a survey. Neural Comput Appl 33:10881–10907. https://doi.org/10.1007/s00521-020-05529-8

Martha TR, Kerle N, Van Westen CJ et al (2011) Segment optimization and data-driven thresholding for knowledge-based landslide detection by object-based image analysis. IEEE Trans Geosci Remote Sens 49:4928–4943. https://doi.org/10.1109/TGRS.2011.2151866

McColl ST (2015) Chapter 2 - landslide causes and triggers. In: Shroder JF, Davies T (eds) Landslide Hazards, Risks, and Disasters. Academic Press, Boston, pp 17–42

Meena SR, Soares LP, Grohmann CH et al (2022) Landslide detection in the Himalayas using machine learning algorithms and U-Net. Landslides 19:1209–1229. https://doi.org/10.1007/s10346-022-01861-3

Milletari F, Navab N, Ahmadi S-A (2016) V-net: Fully convolutional neural networks for volumetric medical image segmentation. In: 2016 fourth international conference on 3D vision (3DV). IEEE, pp 565–571

Mohan A, Singh AK, Kumar B, Dwivedi R (2021) Review on remote sensing methods for landslide detection using machine and deep learning. Trans Emerg Telecom Technol 32:e3998. https://doi.org/10.1002/ett.3998

Mondini AC, Guzzetti F, Reichenbach P et al (2011) Semi-automatic recognition and mapping of rainfall induced shallow landslides using optical satellite images. Remote Sens Environ 115:1743–1757. https://doi.org/10.1016/j.rse.2011.03.006

Oktay O, Schlemper J, Folgoc LL et al (2018) Attention u-net: learning where to look for the pancreas. arXiv preprint. arxiv.org/abs/1804.03999

Ozaki M, Taku K (2014) 1: 200,000 land geological map in the Ishikari depression and its surrounding area with explanatory note. Seamless Geoinformation of coastal zone "southern coastal zone of the Ishikari depression", seamless geological map of costal zone S-4, Geological Survey of Japan ALST

Peng C, Zhang X, Yu G et al (2017) Large kernel matters–improve semantic segmentation by global convolutional network. In: Proceedings of the IEEE conference on computer vision and pattern recognition. pp 4353–4361

Peng F, Lu W, Tan W et al (2022) Multi-output network combining GNN and CNN for remote sensing scene classification. Remote Sensing 14:1478. https://doi.org/10.3390/rs14061478

Phan TH, Yamamoto K (2020) Resolving class imbalance in object detection with weighted cross entropy losses. arXiv preprint, arxiv.org/abs/2006.01413

Puente-Sotomayor F, Egas A, Teller J (2021) Land policies for landslide risk reduction in Andean cities. Habit Intern 107:102298. https://doi.org/10.1016/j.habitatint.2020.102298

Redmon J, Divvala S, Girshick R, Farhadi A (2016) You only look once: unified, real-time object detection. In: Proceedings of the IEEE conference on computer vision and pattern recognition. pp 779–788

Ren S, He K, Girshick R, Sun J (2015) Faster r-cnn: towards real-time object detection with region proposal networks. Adv Neur Inform Proc Syst 28

Roccati A, Paliaga G, Luino F et al (2021) GIS-based landslide susceptibility mapping for land use planning and risk assessment. Land 10:162. https://doi.org/10.3390/land10020162

Ronneberger O, Fischer P, Brox T (2015) U-net: convolutional networks for biomedical image segmentation. In: International Conference on Medical image computing and computer-assisted intervention. Springer, pp 234–241

Stumpf A, Kerle N (2011) Object-oriented mapping of landslides using random forests. Remote Sens Environ 115:2564–2577. https://doi.org/10.1016/j.rse.2011.05.013

Su Z, Chow JK, Tan PS et al (2021) Deep convolutional neural network–based pixel-wise landslide inventory mapping. Landslides 18:1421–1443. https://doi.org/10.1007/s10346-020-01557-6
Sun X, Wang P, Wang C et al (2021) PBNet: Part-based convolutional neural network for complex composite object detection in remote sensing imagery. ISPRS J Photogramm Remote Sens 173:50–65. https://doi.org/10.1016/j.isprsjprs.2020.12.015
Taalab K, Cheng T, Zhang Y (2018) Mapping landslide susceptibility and types using random forest. Big Earth Data 2:159–178. https://doi.org/10.1080/20964471.2018.1472392
Tang X, Ma Q, Zhang X et al (2021) Attention consistent network for remote sensing scene classification. IEEE Journal of Selected Topics in Applied Earth Observations and Remote Sensing 14:2030–2045. https://doi.org/10.1109/JSTARS.2021.3051569
Tavakkoli Piralilou S, Shahabi H, Jarihani B et al (2019) Landslide detection using multi-scale image segmentation and different machine learning models in the higher himalayas. Remote Sensing 11:2575. https://doi.org/10.3390/rs11212575
Tsangaratos P, Ilia I (2016) Comparison of a logistic regression and Naïve Bayes classifier in landslide susceptibility assessments: The influence of models complexity and training dataset size. CATENA 145:164–179. https://doi.org/10.1016/j.catena.2016.06.004
Ullo SL, Mohan A, Sebastianelli A et al (2021) A new mask R-CNN-based method for improved landslide detection. IEEE Journal of Selected Topics in Applied Earth Observations and Remote Sensing 14:3799–3810. https://doi.org/10.1109/JSTARS.2021.3064981
Wang L-J, Sawada K, Moriguchi S (2013) Landslide susceptibility analysis with logistic regression model based on FCM sampling strategy. Comput Geosci 57:81–92. https://doi.org/10.1016/j.cageo.2013.04.006
Wei R, Ye C, Sui T et al (2022) Combining spatial response features and machine learning classifiers for landslide susceptibility mapping. Intern J Appl Earth Observ Geoinform 107:102681. https://doi.org/10.1016/j.jag.2022.102681
Woo S, Park J, Lee J-Y, Kweon IS (2018) Cbam: convolutional block attention module. In: Proceedings of the European conference on computer vision (ECCV). pp 3–19
Wu Q (2020) geemap: a Python package for interactive mapping with Google Earth Engine. J Open Sour Soft 5:2305. https://doi.org/10.21105/joss.02305
Yang Z, Xu C, Li L (2022) Landslide detection based on ResU-Net with transformer and CBAM embedded: two examples with geologically different environments. Remote Sensing 14:2885. https://doi.org/10.3390/rs14122885
Yi Y, Zhang W (2020) A new deep-learning-based approach for earthquake-triggered landslide detection from single-temporal RapidEye satellite imagery. IEEE Journal of Selected Topics in Applied Earth Observations and Remote Sensing 13:6166–6176. https://doi.org/10.1109/JSTARS.2020.3028855
Ye C, Li Y, Cui P et al (2019) Landslide detection of hyperspectral remote sensing data based on deep learning with constrains. IEEE Journal of Selected Topics in Applied Earth Observations and Remote Sensing 12:5047–5060. https://doi.org/10.1109/JSTARS.2019.2951725
Yu B, Chen F (2017) A new technique for landslide mapping from a large-scale remote sensed image: a case study of Central Nepal. Comput Geosci 100:115–124. https://doi.org/10.1016/j.cageo.2016.12.007
Yu B, Xu C, Chen F et al (2022) HADeenNet: a hierarchical-attention multi-scale deconvolution network for landslide detection. Intern J Appl Earth Observ Geoinform 111:102853. https://doi.org/10.1016/j.jag.2022.102853
Yuan Q, Shen H, Li T et al (2020) Deep learning in environmental remote sensing: achievements and challenges. Rem Sens Environ 241:111716. https://doi.org/10.1016/j.rse.2020.111716
Zakria Z, Deng J, Kumar R et al (2022) Multiscale and direction target detecting in remote sensing images via modified YOLO-v4. IEEE Journal of Selected Topics in Applied Earth Observations and Remote Sensing 15:1039–1048. https://doi.org/10.1109/JSTARS.2022.3140776
Zhang S, Li R, Wang F, Iio A (2019) Characteristics of landslides triggered by the 2018 Hokkaido Eastern Iburi earthquake, Northern Japan. Landslides 16:1691–1708. https://doi.org/10.1007/s10346-019-01207-6
Zhao H, Shi J, Qi X et al (2017a) Pyramid scene parsing network. In: Proceedings of the IEEE conference on computer vision and pattern recognition. pp 2881–2890
Zhao W, Li A, Nan X et al (2017b) Postearthquake landslides mapping from Landsat-8 data for the 2015 Nepal earthquake using a pixel-based change detection method. IEEE Journal of Selected Topics in Applied Earth Observations and Remote Sensing 10:1758–1768. https://doi.org/10.1109/JSTARS.2017.2661802
Zhu Q, Guo X, Deng W et al (2022) Land-use/land-cover change detection based on a Siamese global learning framework for high spatial resolution remote sensing imagery. ISPRS J Photogramm Remote Sens 184:63–78. https://doi.org/10.1016/j.isprsjprs.2021.12.005

Wei Lu · Yunfeng Hu (✉) · Zuopei Zhang · Wei Cao
State Key Laboratory of Resources and Environmental Information System, Institute of Geographic Sciences and Natural Resources Research, Chinese Academy of Sciences, Beijing 100101, China
Email: huyf@lreis.ac.cn

Wei Lu · Yunfeng Hu · Zuopei Zhang · Wei Cao
College of Resources and Environment, University of Chinese Academy of Sciences, Beijing 100049, China

Wei Lu
Email: luwei221@mails.ucas.ac.cn

Zuopei Zhang
Email: zhangzuopei19@mails.ucas.ac.cn

Wei Cao
Email: caowei@igsnrr.ac.cn